Eur Biophys J (2005) 34: 1066–1070
DOI 10.1007/s00249-005-0481-0

BIOPHYSICS LETTER

**Veronika Kralj-Iglič · Henry Hägerstrand
Peter Veranič · Kristijan Jezernik · Blaž Babnik
Dorit R. Gauger · Aleš Iglič**

Amphiphile-induced tubular budding of the bilayer membrane

Received: 3 January 2005 / Accepted: 28 February 2005 / Published online: 5 July 2005

Abstract Amphiphile-induced tubular budding of the erythrocyte membrane was studied using transmission electron microscopy. No chiral patterns of the intramembraneous particles were found, either on the cylindrical buds, or on the tubular nanoexovesicles. In agreement with these observations, the tubular budding may be explained by in-plane ordering of anisotropic membrane inclusions in the buds where the difference between the principal membrane curvatures is very large. In contrast to previously reported theories, no direct external mechanical force is needed to explain tubular budding of the bilayer membrane.

Keywords Tubular budding · Amphiphiles · Nanotubes · Freeze-fracture electron microscopy · Deviatoric elasticity

V. Kralj-Iglič
Institute of Biophysics, Faculty of Medicine,
University of Ljubljana, Lipičeva 2, 1000 Ljubljana,
Slovenia

H. Hägerstrand
Department of Biology, Åbo Akademi University, Åbo/Turku,
Finland

P. Veranič · K. Jezernik
Institute of Cell Biology, Faculty of Medicine,
University of Ljubljana, Lipičeva 2, 1000 Ljubljana, Slovenia

V. Kralj-Iglič · B. Babnik · A. Iglič (✉)
Laboratory of Physics, Faculty of Electrical Engineering,
University of Ljubljana, Tržaška 25, 1000 Ljubljana,
Slovenia
E-mail: ales.iglic@fe.uni-lj.si
Tel.: +386-1-4768825
Fax: +386-1-4768850

D. R. Gauger
Friedrich Schiller University, Neugasse 25,
Jena, 07745, Germany

Introduction

Amphiphilic molecules embed readily into the red blood cell membrane thereby causing cell shape changes. When red blood cells reach the echinocytic shape of type III, budding and nanoexovesicle release from the membrane surface start. Most of the amphiphilic molecules studied mainly induce spherical budding and nanoexovesicles, while strongly anisotropic amphiphiles (e.g., dimeric detergents) were found to induce mainly tubular buds and tubular nanoexovesicles (Kralj-Iglič et al. 2000, and references therein). Tubular budding induced by the interaction of amphiphilic molecules (proteins) with the phospholipid bilayer has also been observed in giant phospholipid vesicles (Yamashita et al. 2002; Tsafrir et al. 2003), where an increased local concentration of amphiphiles on the buds has been noted (Tsafrir et al. 2003). Apparently, the tubular budding of erythrocyte membrane and giant phospholipid vesicle membrane described does not need any additional external driving force (Derényi et al. 2002).

In the past, tubular budding of the erythrocyte membrane was observed (Lutz et al. 1977) in sheep erythrocytes aged in vitro. In released tubular nanoexovesicles the freeze-fracture method revealed a spiral-like arrangement of intramembraneous particles (IMP) that is in agreement with the mechanism of tubular budding based on the chirality associated with the membrane constituents (Selinger et al. 1996). We were interested to find out whether such chiral structures can also be observed in our detergent-induced tubular buds of the human erythrocyte membrane. Our results show no evidence for chiral structures on the tubular buds/vesicles. Accordingly, we propose a possible explanation for the observed nanotubular budding of the erythrocyte membrane that is based on the orientational ordering of anisotropic membrane constituents (Fournier 1996). The proposed theoretical description is also applicable to the description of the amphiphile-induced tubular budding in giant phospholipid vesicles, where tubulation occurs

without an external mechanical force (Yamashita et al. 2002; Tsafrir et al. 2003).

Materials and methods

Incubation of red blood cells

Human blood was drawn from healthy volunteers (the authors) by venous puncture into heparinized tubes. After washing, the red blood cells were pipetted into polystyrene tubes containing a buffer with dodecylmaltoside (Fluka, Buchs, Switzerland). The final cell density was 1.65×10^8 cells/ml (about 1.5% haematocrit) and incubation was carried out at 37°C for 60 min. Dodecylmaltoside was used at a sublytic concentration (40 μM).

Transmission electron microscopy of cells following freeze fracturing

The cells were fixed in 2.5% glutaraldehyde and 4% paraformaldehyde in 0.1 M cacodylate buffer, pH 7.3, for 2 h at 4°C. Fixed cells were soaked in 30% glycerol in 0.1 M cacodylate buffer for at least 2 h before being frozen in liquid Freon 22. Freeze-fracture replicas were produced in a Balzers freeze-fracture unit and were examined using a JEOL 100 CX transmission electron microscope.

Transmission electron microscopy of dried samples containing nanovesicles

After incubation with dodecylmaltoside cells were pelleted by centrifugation at 1,400*g* for 10 min. The nanoexovesicles, after an additional centrifugation of the supernatant as described before, were pelleted by centrifugation of the resulting supernatant at 20,000*g* for 40 min. The nanoexovesicles were fixed in 2% glutaraldehyde in buffer for 60 min and postfixed in 1% OsO_4 in buffer for 30 min. A drop containing fixed nanoexovesicles was applied on a formvar-coated grid. After short drying, nanoexovesicles were examined with the JEOL 100 CX transmission electron microscope.

Experimental results

In the process of transformation of the red blood cell from a discocyte shape to a shape composed of a mother-cell and the released microexovesicles, owing to continuous intercalation of dodecylmaltoside molecules into the membrane the red blood cell first undergoes a discocyte–echinocyte transformation. Then budding occurs at the top of the echinocyte spicules. Figure 1a shows a tubular bud on top of the echinocyte spicule, while Fig. 1b apparently shows a released tubular nanoexovesicle as observed by transmission electron microscopy (TEM) of freeze-fracture replicas. We inspected tens of TEM micrographs of tubular buds and tubular nanovesicles and did not find any with a chiral IMP arrangement.

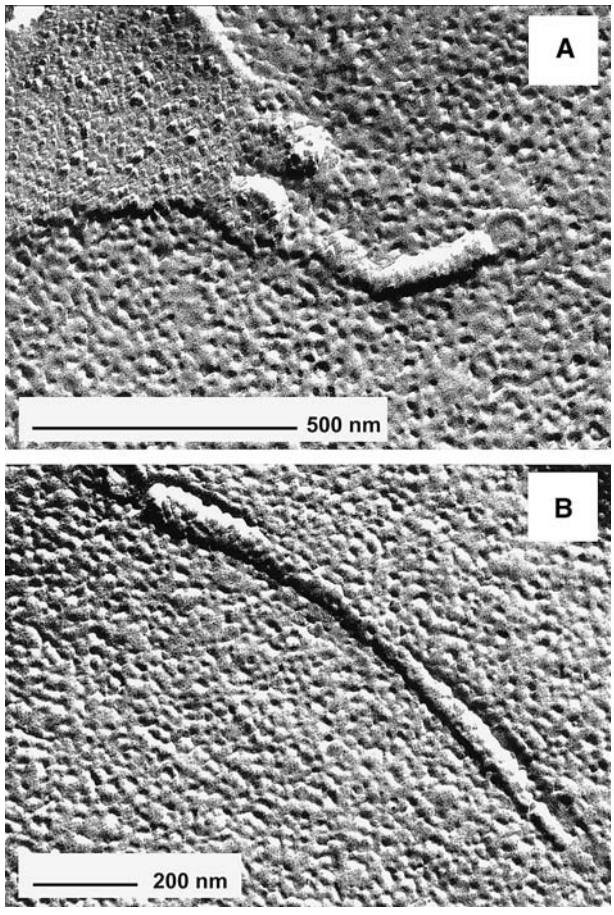

Fig. 1 Transmission electron microscopy (*TEM*) micrographs of freeze-fracture replicas showing the tubular bud on top of the echinocyte spicule (**a**) and the free tubular nanoexovesicle released from the membrane (**b**). The budding/vesiculation was induced by adding 40 μM dodecylmaltoside to the erythrocyte suspension. No chiral arrangement of intramembraneous particles can be observed

To obtain a better insight into the shape of the released tubular nanoexovesicles, the nanovesicles were observed directly by TEM (Fig. 2). Figure 2 confirms that the nanovesicles are tubular. Some very long tubular nanovesicles can be seen.

Theoretical discussion

Protein analysis showed that the released spherical and tubular daughter nanovesicles of the erythrocyte membrane are highly depleted in the membrane skeleton (Hägerstrand et al. 1999), and therefore the shape of the buds/vesicles is determined by the properties of the membrane bilayer. It is of interest to understand the mechanisms which determine the observed amphiphile-

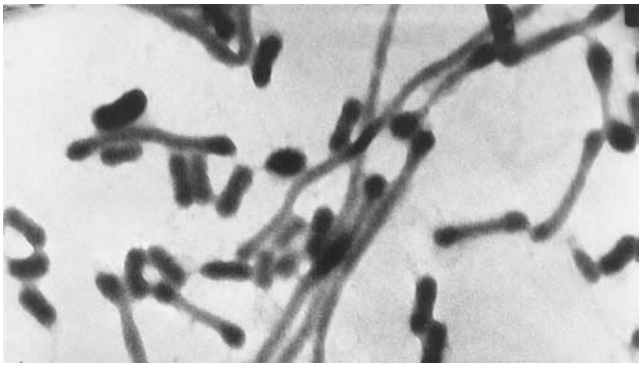

Fig. 2 TEM micrographs of dried samples showing released tubular nanoexovesicles induced by adding 40 μM dodecylmaltoside to the erythrocyte suspension

induced tubular budding of the bilayer membrane (Fig. 1a). The bilayer couple hypothesis and the standard area difference–elasticity (ADE) model (Sheetz and Singer 1974; Evans 1974; Helfrich 1974; Miao et al. 1994) that is based on the description of the membrane as a bilayer composed of two compressible isotropic monolayers (Helfrich 1974; Evans and Skalak 1980; Stokke et al. 1986) does not provide an explanation for tubular budding if no pulling force is applied (Miao et al. 1991, 1994; Derényi et al. 2002; Tsafrir et al. 2003). Within the ADE model stable shapes were determined by minimizing the Helfrich–Evans membrane bending energy (Evans and Skalak 1980; Helfrich 1974; Stokke et al. 1986; Miao et al. 1994):

$$W_b = \frac{k_c}{2}\int (2H)^2 dA + k_n A(\langle H\rangle - H_0)^2, \qquad (1)$$

where $\langle H\rangle = \left(\int H\,dA\right)/A$ is the average mean curvature, H is the local mean curvature, H_0 is the effective spontaneous mean curvature (Mukhopadhyay et al. 2002), k_c is the membrane isotropic bending constant, k_n is the coefficient of nonlocal bending rigidity (Evans and Skalak 1980), A is the membrane area and d A is the area element. For thin and not too strongly curved bilayers the average mean curvature $\langle H\rangle$ is proportional to the area difference between the two membrane monolayers: $(\Delta A) : \langle H\rangle = \Delta A/2A\delta$, where δ is the distance between the two monolayer neutral surfaces.

A possible physical mechanism that may yield an explanation for tubular budding can be based on the chirality associated with the membrane constituents (Selinger et al. 1996). Such structures were observed in sheep erythrocytes aged in vitro (Lutz et al. 1977). However, in our samples we did not observe a single tubular bud or a nanovesicle showing a chiral pattern of IMP organization. Therefore, we suggest that the driving mechanism of the observed tubular budding is based on orientational ordering of the detergent-induced membrane inclusions (Fournier 1996) in the erythrocyte membrane. The free energy of the membrane with anisotropic inclusions is (Kralj-Iglič et al. 1999)

$$F = W_b - MkT\ln\left[\frac{1}{A}\int q_c I_0\left(\frac{\xi+\xi^*}{2kT}DD_m\right)dA\right], \qquad (2)$$

where $q_c = \exp\left[-\xi(H-H_m)^2\Big/2kT - (\xi+\xi^*)\right.$ $\left.(D^2+D_m^2)\Big/4kT\right]M$ is the total number of inclusions in the outer lipid layer, kT is the thermal energy, ξ and ξ^* are the interaction constants, H_m is the mean curvature intrinsic to the inclusion, D is the local curvature deviator and D_m is the curvature deviator intrinsic to the inclusion (Fournier 1996; Kralj-Iglič et al. 1996; Iglič et al. 2004). For isotropic inclusions $D_m = 0$, while for anisotropic inclusions $D_m \neq 0$. Introducing the dimensionless quantities, we can normalize the energy F by $8\pi k_c$:

$$f = \frac{1}{4}\int (2h)^2 da + \frac{k_n}{2k_c}(\langle h\rangle - h_0)^2 - \frac{MkT}{8\pi k_c}\ln\left[\int q_c I_0\left(\frac{\xi dd_m}{kTR_0^2}\right)da\right], \qquad (3)$$

where $q_c = \exp\left\{-\xi\left[(h-h_m)^2 - d^2 - d_m^2\right]\Big/2kTR_0^2\right\}$. We assumed $\xi = \xi^* \sim 5000kT$ nm^2 (Iglič et al. 2004). The normalized quantities are defined as $h = R_0H$, $h_0 = R_0H_0$, $d = R_0D$, $h_m = R_0H_m$, $d_m = R_0D_m$, $\langle h\rangle = R_0\langle H\rangle$ and $da = dA/4\pi R_0^2$, where $R_0 = \sqrt{A/4\pi}$. The normalized average mean curvature $\langle h\rangle$ is equal to the normalized area difference: $\Delta a = \Delta A/8\pi\delta R_0$.

In the following it will be shown that anisotropic membrane inclusions can induce tubular budding. For the sake of simplicity we shall compare the membrane free energy F only for two limit shapes (for the definition of the limit shapes see Iglič et al. 1999, and references therein). The first limit shape (shape 1) is composed of a spherical mother cell with radius R_s and a bud (protrusion) composed of N small spheres with radius r_s connected by infinitesimal necks. The second limit shape (shape 2) is composed of a spherical mother cell with radius R_c and a thin tube with radius r_c and length l_c which is closed by hemispherical caps (Fig. 3). Each of these two limit shapes involves three geometrical parameters. From the geometrical constraints for the normalized cell volume $v = 3V/4\pi R_0^3$, the normalized cell area $a = A/4\pi R_0^2 = 1$, and the normalized average mean curvature of the cell membrane $\langle h\rangle$, the values (measured in units of R_0) of the three geometrical parameters for each of the two limit shapes can be determined numerically as a function of v and $\langle h\rangle$. Thus, at a given normalized cell volume v the membrane free energy f (Eq. 3) can be calculated as a function of $\langle h\rangle$.

For given values of the normalized cell volume v, h_0, d_m and h_m, the membrane free energies f of both limit shapes were minimized as a function of $\langle h\rangle$, so the equilibrium shapes (corresponding to the absolute minima of f over all possible $\langle h\rangle$ values) were found. Then the equilibrium energies of both limit shapes (1 and 2) were compared to discover which equilibrium limit shape (1 or 2) yields the lowest possible f at the chosen values of v, M and d_m, where we assumed $d_m = h_m$. Since the normalized spontaneous mean curvature h_0 depends on the total number of membrane inclusions in the outer layer M,

$$h_0 = h_{0,\mathrm{ref}} + \frac{Ma}{8\pi\delta R_0}, \tag{4}$$

where a is the average area of the inclusion, the procedure described enables us to draw the (d_m, M) phase diagram of the equilibrium cell shapes with buds for a chosen value of v (Fig. 3).

It can be seen in Fig. 3 that tubular budding may be energetically favourable if the total number of anisotropic inclusions in the outer membrane layer (M) is large enough. For smaller M the tubular bud is shorter and broader since the spontaneous mean curvature h_0 is smaller (see Eq. 4) and consequently also the equilibrium value of $\langle h \rangle$ is smaller, meaning that the buds are shorter and broader. In line with experimental observations (Corbeil et al. 2001; Hägerstrand et al. 1999; Tsafrir et al. 2003), the increased local concentration of inclusions on the buds has also been predicted. On the other hand, without the anisotropic inclusions in the membrane bilayer model, spherical budding is always energetically favourable (Fig. 3). This result is in accordance with the results of previous studies which show that within the standard ADE model there is no evidence that tubular budding is energetically the most favourable without the direct pulling mechanical force (Miao et al. 1991, 1994; Derényi et al. 2002; Tsafrir et al. 2003).

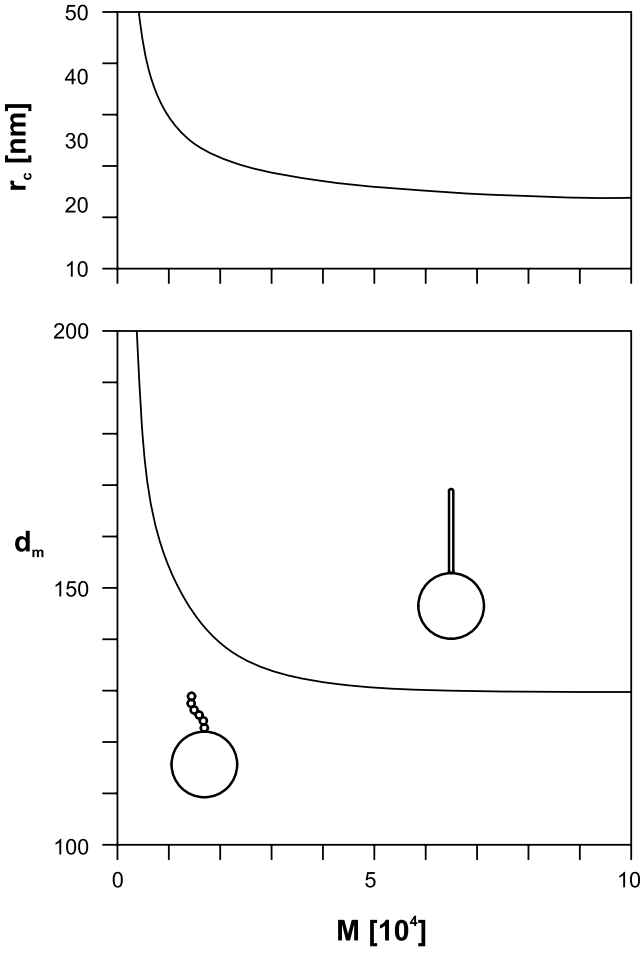

Fig. 3 A (d_m, M) phase diagram of calculated equilibrium cell shapes with beadlike and tubular buds. The regions where spherical or tubular budding is energetically more favourable are indicated. The figure also shows the value of the radius of the tubular bud (r_c) on the *line* separating the two phases. The model parameters used in calculations were $v = 0.95$, $h_{0,\mathrm{ref}} = 1$, $h_m = d_m$, $\delta = 3$ nm, $\xi/2kTR_0^2 = 0.0005$ ($R_0 = 3$ μm), $k_c = 20kT$, $k_n/k_c = 6$ (Hwang and Waugh 1997)

Tubular budding has already been observed in the case of tubular exovesiculation induced by dimeric detergents (Kralj-Iglič et al. 2000). In dimeric detergents, two units, each composed of a head and a tail, are joined by a spacer at the headgroup level. Such a structure is clearly strongly anisotropic with respect to the axis pointing in the direction of the membrane normal (Fournier 1996). In dodecylmaltoside, there is a single tail and a large bulky headgroup composed of two units, so that it is possible that in dodecylmaltoside the anisotropy derives from the headgroup. However, it is also possible that owing to interactions of dodecylmaltoside with the membrane constituents anisotropic protein–detergent complexes or anisotropic lipid–detergent clusters (Fournier 1996) are formed.

Conclusions

The results of some recent studies indicated that thin tubular membraneous structures are common and important in cell structure and function (Iglič et al. 2003; Rustom et al. 2004), but they have not been extensively explored in the past because of the experimental difficulties in investigating these thin and fragile structures. Experiments show that adding amphiphilic molecules (detergents) to an erythrocyte suspension induces budding; the buds may be spherical or tubular. The shape of the buds depends on the intrinsic shape of the detergents added or detergent-induced inclusions.

Our observations reveal that tubular budding can be induced by adding an amphiphilic detergent (dodecylmaltoside) to the erythrocyte suspension. No chiral patterns of the IMP were found, either on the the cylindrical buds or on the tubular nanoexovesicles released. We showed that the observed amphiphile-induced tubular budding can be theoretically explained by in-plane orientational ordering (Fournier 1996) and accumulation of anisotropic membrane inclusions in the budding region. In contrast to some previously reported theories, no direct pulling mechanical force, which is one of the possible driving forces of membrane tubulation in biological systems (Derényi et al. 2002), is needed to explain the observed feature. In line with our theoretical prediction it was recently shown that plasma membrane protrusions (microvilli, filopodia, microspikes) exhibit a specific membrane protein and lipid composition and organization which differs from that of the planar region of the plasma membrane (Corbeil et al. 2001).

In the ADE model (Miao et al. 1994; Seifert and Lipowsky 1995;Mukhopadhyay et al. 2002) the equilibrium vesicle shapes depend on the normalized cell volume v and on the normalized effective spontaneous average mean curvature h_0. In this work we proposed an extension of the phase diagram of the ADE model into the dimension of the normalized intrinsic curvature deviator d_m. The proposed extension of the phase diagram of vesicle shapes in the third dimension (in the direction of the coordinate d_m as shown in Fig. 3) represents a generalization of the bilayer couple hypothesis and the ADE model (Sheetz and Singer 1974; Evans 1974; Helfrich 1974; Miao et al. 1994) which is necessary in order to include in the phase diagram stable shapes having a very large difference between the principal membrane curvatures, for example vesicle shapes with nanotubular protrusions and shapes with very thin necks.

Acknowledgements Stimulating discussions with Hans U. Lutz and Sylvio May are gratefully acknowledged. The Åbo Akademy University supported the stay of A.I. at Åbo Akademy University in Åbo/Turku.

References

Corbeil D, Röper K, Fargeas CA, Joester A, Huttner WB (2001) Prominin: a story of cholesterol, plasma membrane protrusions and human pathology. Traffic 2:82–91

Derényi I, Jülicher F, Prost J (2002) Formation and interaction of membrane tubes. Phys Rev Lett 88:238101/1–4

Evans E (1974) Bending resistance and chemically induced moments in membrane bilayers. Biophys J 14:923–931

Evans EA, Skalak R (1980) Mechanics and thermodynamics of biomembranes. CRC Press, Boca Raton

Fournier JB (1996) Nontopological saddle-splay and curvature instabilities from anisotropic membrane inclusions. Phys Rev Lett 76:4436–4439

Hägerstrand H, Kralj-Iglič V, Bobrowska-Hägerstrand M, Iglič A (1999) Membrane skeleton detachment in spherical and cylindrical microexovesicles. Bull Math Biol 61:1019–1030

Helfrich W (1974) Blocked lipid exchange in bilayers and its possible influence on the shape of vesicles. Z Naturforsch 29c:510–515

Hwang WC, Waugh RE (1997) Energy of dissociation of lipid bilayer from the membrane skeleton of red cells. Biophys J 72:2669–2678

Iglič A, Kralj-Iglič V, Majhenc J (1999) Cylindrical shapes of closed lipid bilayer structures correspond to an extreme area difference between the two monolayers of the bilayer. J Biomech 32:1343–1347

Iglič A, Hägerstrand H, Bobrowska-Hägerstrand M, Arrigler V, Kralj-Iglič V (2003) Possible role of phospholipid nanotubes in directed transport of membrane vesicles. Phys Lett A 310:493–497

Iglič A, Fošnarič M, Hägerstrand H, Kralj-Iglič V (2004) Coupling between vesicle shape and the non-homogeneous lateral distribution of membrane constituents in Golgi bodies. FEBS Lett 574(1–3):9–12

Kralj-Iglič V, Svetina S, Žekš B (1996) Shapes of bilayer vesicles with membrane embedded molecules. Eur Biophys J 24:311–321

Kralj-Iglič V, Heinrich V, Svetina S, Žekš B (1999) Free energy of closed membrane with anisotropic inclusions. Eur Phys J B 10:5–8

Kralj-Iglič V, Iglič A, Hägerstrand H, Peterlin P (2000) Stable tubular microexovesicles of the erythrocyte membrane induced by dimeric amphiphiles. Phys Rev E 61:4230–4234

Lutz HU, Lomant AJ, McMillan P, Wehrli E (1977) Rearrangements of integral membrane components during in vitro aging of sheep erythrocyte membranes. J Cell Biol 74:389–398

Miao L, Fourcade B, Rao M, Wortis M, Zia RKP (1991) Equilibrium budding and vesiculation in the curvature model of fluid lipid vesicles. Phys Rev E 43:6843–6856

Miao L, Seifert U, Wortis M, Döbereiner HG (1994) Budding transitions of fluid-bilayer vesicles: effect of area difference elasticity. Phys Rev E 49:5389–5407

Mukhopadhyay R, Lim G, Wortis M (2002) Echinocyte shapes: bending, stretching and shear determine spicule shape and spacing. Biophys J 82:1756–1772

Rustom A, Saffrich R, Markovič I, Walther P, Gerdes HH (2004) Nanotubular highways for intercellular organelle transport. Science 303:1007–1010

Seifert U, Lipowsky R (1995) Morphology of vesicles. In: Lipowsky R, Sackmann E (eds) Structure and dynamics of membranes. From cells to vesicles. Elsevier, Amsterdam, pp 403–463

Selinger JV, MacKintosh FC, Schnur JM (1996) Theory of cylindrical tubules and helical ribbons of chiral lipid membranes. Phys Rev E 53:3804–3818

Sheetz MP, Singer SJ (1974) Biological membranes as bilayer couples. A molecular mechanism of drug-erythrocyte interactions. Proc Natl Acad Sci USA 71:4457–4461

Stokke BT, Mikkelsen A, Elgsaeter A (1986) The human erythrocyte membrane skeleton may be an ionic gel. Eur Biophys J 13:203–218

Tsafrir I, Caspi Y, Guedeau MA, Arzi T, Stavans J (2003) Budding and tubulation of highly oblate vesicles by anchored amphiphilic molecules. Phys Rev Lett 91:138102/1–4

Yamashita Y, Masum SM, Tanaka T, Tamba Y, Yamazaki M (2002) Shape changes of giant unilamellar vesicles of phosphatidylcholine induced by a de novo designed peptide interacting with their membrane interface. Langmuir 18:9638–9641